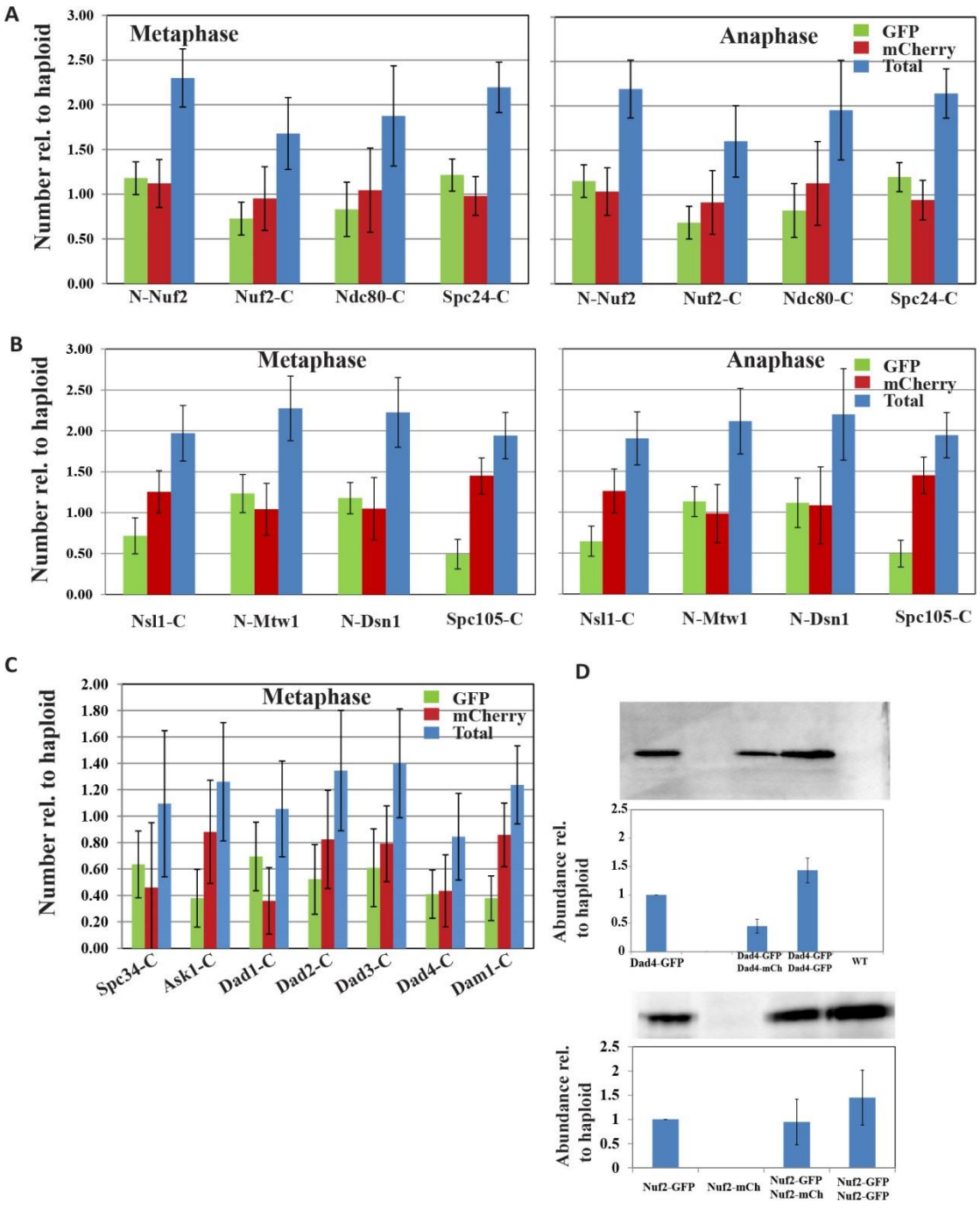

Figure S1 – Relative abundance of GFP and mCherry-labeled kinetochore proteins in heterozygous diploid strains.

(A) Relative abundance was calculated as the ratio of average fluorescence from kinetochore clusters in diploid strains expressing GFP- and mCherry-fusions of a protein to the average fluorescence for

kinetochore clusters in haploid strains expressing the same subunit fused with either GFP only or mCherry only (mean ± std. dev.; std. dev. calculated using error propagation; [S1]). The ideal value of this ratio is 1. Since diploid kinetochore clusters carry twice as many molecules as haploid clusters, the addition of the two ratios (Total) should then equal 2. Ideal or close to ideal values for these ratios ensure that the kinetochore clusters contain the maximum possible number of FRET pairs [S2].

(B) GFP and mCherry labeled subunits of the Mtw1 complex are recruited in approximately equal numbers. Preferential recruitment of mCherry-labeled protein over the GFP-labeled protein is seen for Nsl1 and Spc105. Due to the preferential recruitment of mCherry-labeled molecules, the actual proximity ratios for these two measurements can be expected to be higher by ~ 25% corresponding to the degree of imbalance in the recruitment. The linear nature of this dependence was experimentally verified in ref. [S2].

(C) Relative abundance of GFP and mCherry labeled Dam1 complex subunits in diploid kinetochore clusters. Only metaphase data is shown, since Dam1 complex partially dissociates from the kinetochore in anaphase and redistributes to the spindle.

(D) Western blot quantitation for the Dam1 complex subunit Dad4-GFP and the Ndc80 complex subunit Nuf2-GFP in haploid, heterozygous diploid (expressing both GFP- and mCherry labeled protein) and homozygous diploid strains (expressing GFP-labeled proteins from both genomic copies). Signal quantitation from three western blots normalized with the haploid signal for each subunit (mean +\- std. dev. displayed). Expression levels for both Nuf2-GFP and Dad4-GFP are higher in homozygous diploid strains. Therefore, protein expression does not explain the significantly lower recruitment of Dam1 complex in diploid strains.

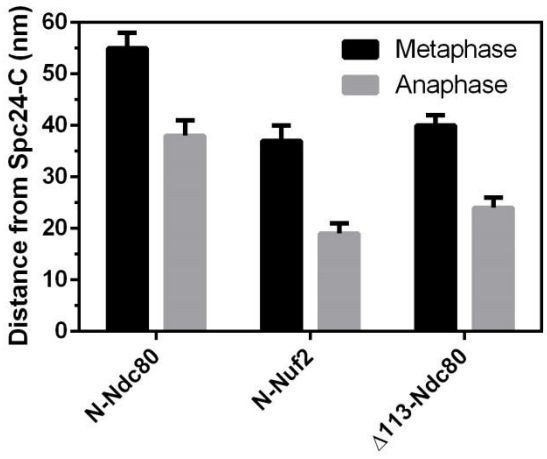

Figure S2 – Comparison of the average projected separation between Spc24-C and Ndc80 subunit termini in metaphase and late anaphase/telophase

Separation between Spc24-C and the indicated subunit termini (mean ± 95% confidence intervals on the mean obtained from maximum likelihood analysis) decreases systematically in late anaphase/telophase, as reported previously [S3]. The separation of only 20 nm does not necessarily suggest that the Ndc80 complex bends at locations other than the flexible kink. Our distance measurements represent the average separations over 16 kinetochores. With centromeric tension absent in late anaphase/telophase, kinetochores are not constrained to remain parallel to the spindle axis. Some of the kinetochores may even lie parallel to the face of the spindle pole body as suggested by serial section electron microscopy [S4]. Kinetochores with this orientation will reduce the *average* separation between labeled domains significantly. In addition tilting of the spindle pole body with respect to the image plane will also reduce the projected separation between N-Nuf2 and Spc24-C.

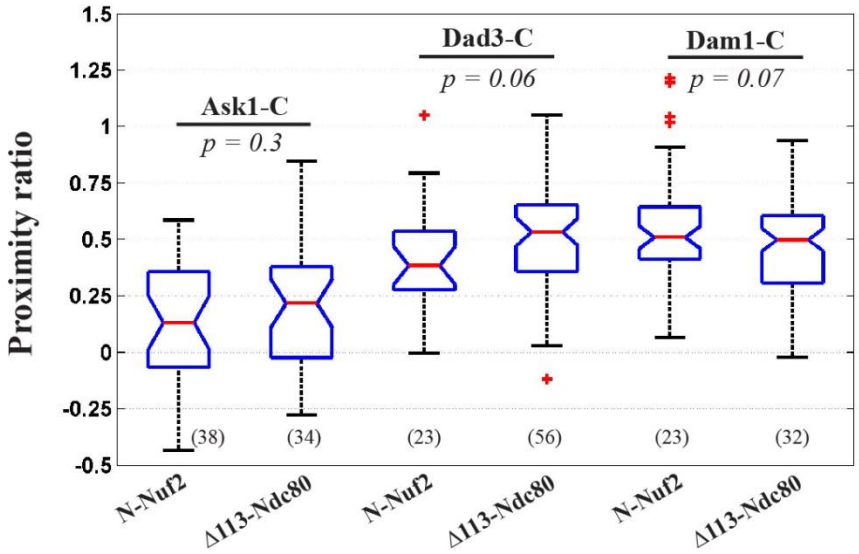

Figure S3 - Proximity of Dam1 subunits to the amino termini of Nuf2 or Δ113-Ndc80. Although the differences in the measured proximity ratios are statistically indistinguishable, the deletion of the MT-binding tail of Ndc80 may perturb the actual distributions.

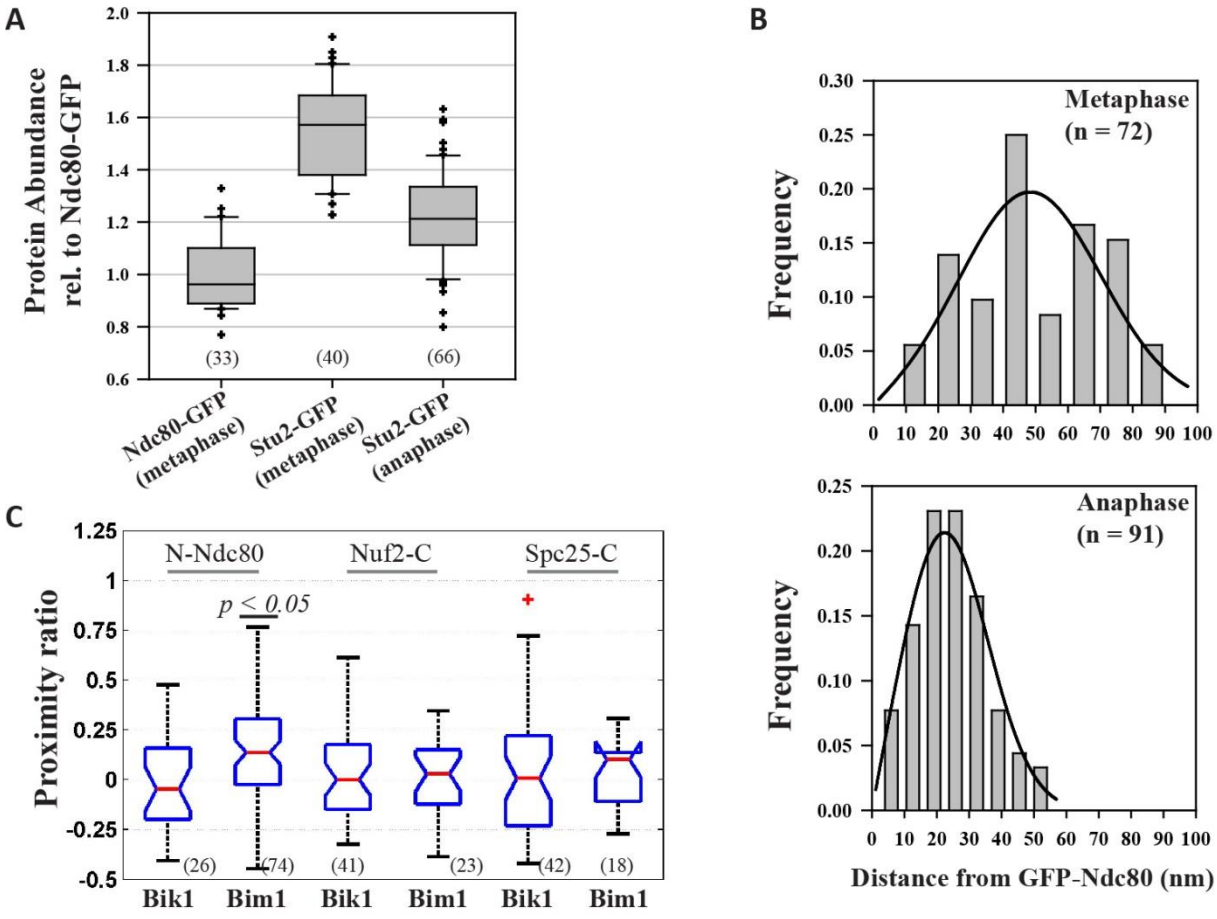

Figure S4 – Nanoscale distributions of MAPs in the metaphase kinetochore

(A) Abundance of Stu2-GFP in metaphase and late anaphase/telophase cells relative to Ndc80-GFP (mean +\- std. dev.). There is a substantial decrease in kinetochore-localized Stu2-GFP in late anaphase/telophase ($p < 10^{-9}$, Student t-test).

(B) Histogram of the separation between GFP-Ndc80 and Stu2-mCherry in metaphase and late anaphase/telophase using High resolution colocalization. Maximum likelihood distribution fitting with a non-Gaussian distribution predicts that Stu2-mCherry is 43 ± 3 nm (n=72) inside (towards the centromere) GFP-Ndc80 (19 ± 2 nm in late anaphase/telophase). This distance places the average position of Stu2 in close vicinity of Nuf2-C or Ndc80-C, which is consistent with FRET measurements (Figure 5C).

(C) FRET between either Bik1-C or Bim1-C and various Ndc80 complex domains. Only the Bim1-C/N-Ndc80 pair allows FRET ($p \sim 0.05$, Wilcoxon rank sum test).

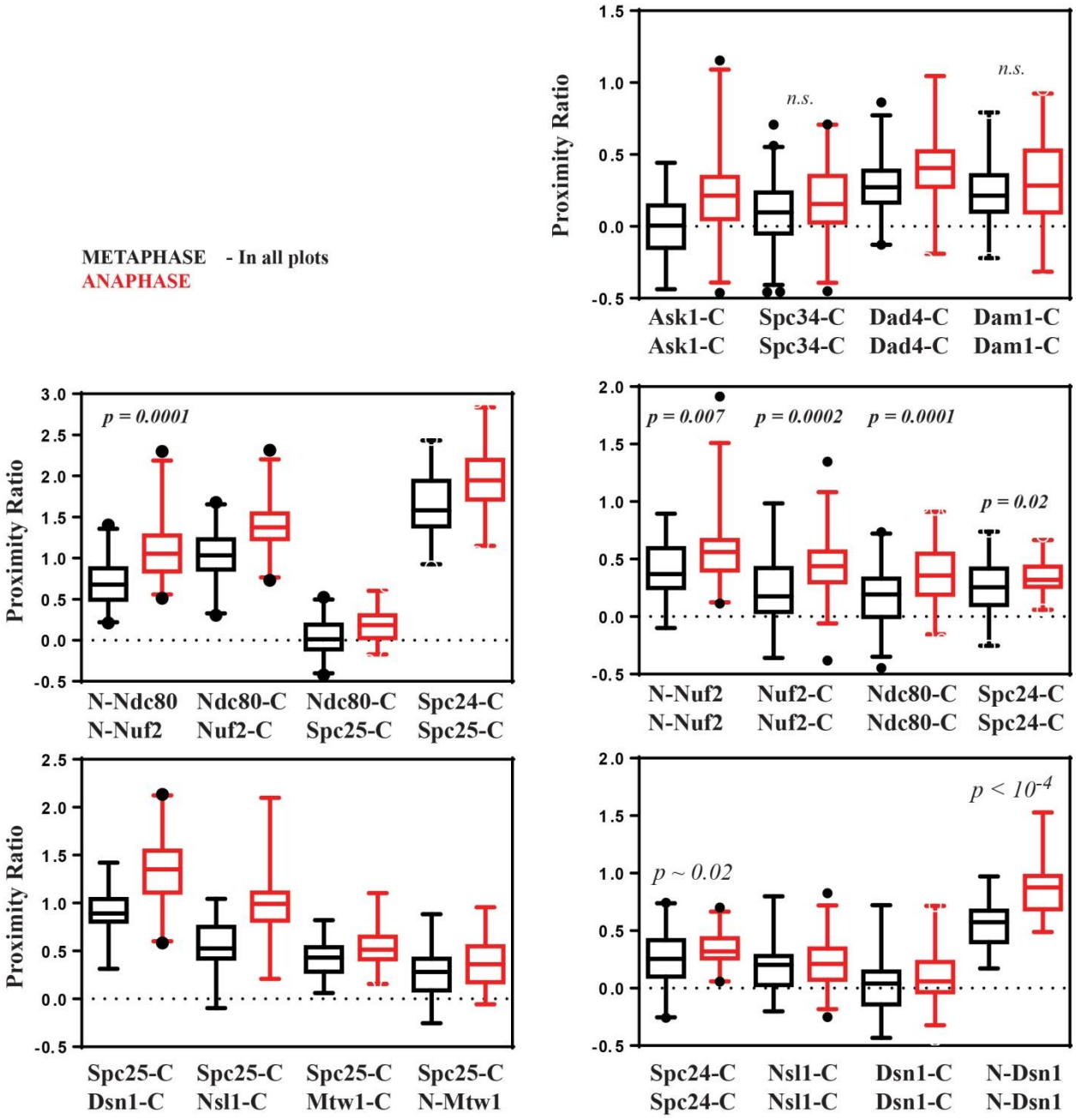

Figure S5 – FRET between kinetochore proteins in late anaphase/telophase is systematically higher than the FRET measured in metaphase. Although the higher FRET suggests an overall compaction of kinetochore subunits, two additional factors may also contribute. First, inter-kinetochore FRET may occur due to the tight clustering of anaphase kinetochores near the spindle pole body [S4]. It should be noted that we use the separation between kinetochore clusters to designate the kinetochore clusters as metaphase and late anaphase/telophase (see Supplemental Methods). It is possible a fraction of previously non-fluorescent mCherry molecules may mature during the intervening time period, and contribute to the increased sensitized emission detected in late anaphase/telophase cells.

Supplementary Note 1

Minimizing the impact of fluorophore size on FRET-based analysis of kinetochore architecture – The large size of GFP and mCherry (3 nm diameter x 4 nm height, with fluorophore located at the center) generally discourages the use of these proteins as a FRET pair, where the donor-acceptor separation is the parameter of interest [S5]. This size can impact the process of FRET in two ways. First, the large size and steric effects may prevent is isotropic rotation of the donor and acceptor. Therefore, differences in FRET efficiency may not necessarily indicate different protein separations. It is important to note that the magnitude of this artifact is considerably dampened by the highly non-linear dependence of FRET efficiency on the relative fluorophore rotation [S6]. We also use a 7 a. a. linker to facilitate fluorophore rotation about the labeled kinetochore protein terminus. As discussed in the manuscript, we verify each key conclusion by using multiple, independent measurements. Therefore, it is unlikely that fluorophore rotation systematically affects our data.

The large size of fluorescent proteins can also either enlarge or diminish the actual separation between labeled termini. It is important to note that each FRET measurement reported here represents an average over hundreds of FRET pairs from many kinetochore clusters. Therefore, it is reasonable to assume that the donor and acceptor fluorescent proteins are as likely to be further away from one another as they are closer to one another. Therefore, the *average* contribution of fluorophore size to the separation will be minimal (provided that the distance being measured is larger than ~ 4 nm, the size of the fluorophores). This expectation regarding the contribution of fluorophore size is supported by the close agreement between *in vivo* projected length of the Ndc80 complex using fluorescent protein tags with its molecular dimensions [S3, S7]. Therefore, that the *average* contribution to the separation being measured is negligible.

We previously determined that the maturation efficiency of mCherry is only 30-50% relative to GFP [S2, S8]. However, inefficient mCherry maturation is systematic to all the reported measurements, and it only lowers the sensitized emission intensity in all the measurements [S2]. It does not affect the comparison of proximity ratios used here.

Table S1 Strains used in this study

Strain #	***Genotype***	***Figure***
AJY1	*MatA, trp1Δ63, leu2Δ, ura3-52, his3Δ200, lys2-8Δ1*	
AJY2	*Matα, trp1Δ63, leu2Δ, ura3-52, his3Δ200, lys2-8Δ1*	
AJY1694	*MatA, prNdc80-GFP-NDC80, NUF2-mCherry:Hyg*	Figure 2
AJY2093	*MatA, prNdc80-GFP::Δ113-ndc80, nat:pGal1-mCherry-NUF2*	Figure 2
AJY872	*MatA, NDC80-GFP:kan, NUF2-mCherry:kan*	Figure 1, 2
AJY939	*MatA, NDC80-GFP:kan, SPC25-mCherry:kan*	Figure 1, 2
AJY836	*MatA, SPC24-GFP:kan, SPC25-mCherry:nat*	Figure 1, 2
AJY2008	*MatA, prNdc80-GFP-NDC80, pGal-mCherry-NUF2:nat*	Figure 2
AJY1304	*MatA, prNdc80-GFP-NDC80, SPC25-mCherry:Hph*	Figure 2
AJY1406	*MatA/Matα, kan::pGal1-GFP-NUF2/kan::pGal1-mCherry-NUF2*	Figure 2
AJY476	*MatA/Matα, NDC80-GFP:TRP1/NDC80-mCherry:Kan*	Figure 2
AJY741	*MatA/Matα, gal2Δ::HIS3/gal2Δ::HIS3, NUF2-GFP:Trp/NUF2-mCherry:kan*	Figure 2
AJY2221	*MatA/Matα, SPC24-GFP:kan/SPC24-ymCherry:Hyg*	Figure 2
AJY1304	*MatA, prNdc80-GFP-NDC80, SPC25-mCherry:Hph*	Figure 2,3
AJY1534	*MatA, prNdc80-GFP-Δ113-ndc80, SPC24-mCherry:Hyg*	Figure 3
AJY2146	*MatA, SPC24-GFP:kan, pGal1-mCherry-GG-NUF2:nat*	Figure 3
AJY868	*MatA/Matα, DAD1-GFP:HIS3/DAD1-mCherry:kan*	Figure 4
AJY869	*MatA/Matα, DAD2-GFP:HIS3/DAD2-mCherry:kan*	Figure 4
AJY1071	*MatA/Matα, DAD3-GFP:kan/DAD3-mCherry:TRP1*	Figure 4
AJY918	*MatA/Matα, DAD4-GFP:kan/DAD4-mCherry:nat*	Figure 4
AJY1370	*MatA/Matα, DAM1-GFP:Kan/DAM1-mCherry:Hyg*	Figure 4
AJY1369	*MatA/Matα, ASK1-GFP:Kan/ASK1-mCherry:Hyg*	Figure 4
AJY1371	*MatA/Matα, SPC34-GFP:Kan/SPC34-mCherry:Hyg*	Figure 4
AJY2092	*MatA, DAM1-GFP:kan, nat:pGal1-mCherry-NUF2*	Figure 4
AJY2145	*MatA, DAD3-GFP:kan, nat:pGal1-mCherry-GG-NUF2*	Figure 4
AJY1496	*MatA, nat:pGal1-GFP-NUF2, ASK1-mCherry:Hyg*	Figure 4
AJY2098	*MatA, SPC34-GFP:kan, nat:pGal1-mCherry-NUF2*	Figure 4
AJY2144	*MatA, DAD1-GFP:kan, pGal1-mCherry-GG-NUF2:nat*	Figure 4
AJY1198	*MatA, prNdc80-GFP:Δ113-ndc80, ASK1-mCherry:kan*	Figure S3
AJY1193	*MatA, prNdc80-GFP:Δ113-ndc80, DAD3-mCherry:kan*	Figure S3
AJY1200	*MatA, prNdc80-GFP:Δ113-ndc80, DAM1-mCherry:kan*	Figure S3
AJY1324	*MatA, NUF2-GFP:Kan,ASK1-mCherry:Hyg*	Figure 4
AJY1326	*MatA, SPC24-GFP:Kan,ASK1-mCherry:Hyg*	Figure 4
AJY842	*MatA, STU2-GFP:kan*	Figure 5
AJY1605	*MatA, STU2-GFP:kan, MTW1-mCherry:Hyg*	Figure 5
AJY1607	*MatA, MTW1-GFP:TRP1, STU2-mCherry:nat*	Figure 5
AJY2157	*MatA, STU2-GFP:kan, pMET3-CDC20:TRP1*	Figure 5
AJY2222	*MatA, STU2-GFP:kan, DAD2-ymCherry:Hyg*	Figure 5

Strain #	***Genotype***	***Figure***
AJY2223	*MatA, STU2-GFP:kan, Spc19-ymCherry:Hyg*	Figure 5
AJY1604	*MatA, STU2-GFP:kan, MTW1-mCherry: Hyg*	Figure 5
AJY838	*MatA, SPC24-GFP:kan, STU2-mCherry:nat*	Figure 5
AJY1254	*MatA, NDC80-GFP:kan, STU2-mCherry:nat*	Figure 5
AJY1603	*MatA, NUF2-GFP:TRP1, STU2-mCherry:Nat*	Figure 5
AJY2179	*MatA, prNdc80-GFP-NDC80, STU2-mCherry:Hyg*	Figure 5
AJY1684	*MatA, prStu2-GFP-STU2, SPC24-mCherry:Hyg*	Figure 5
AJY1692	*MatA, prStu2-GFP-STU2, NUF2-mCherry:Hyg*	Figure 5
AJY1693	*MatA, prStu2-GFP-STU2, MTW1-mCherry:Hyg*	Figure 5
AJY1703	*MatA, prStu2-GFP-STU2, DAD3-mCherry:kan*	Figure 5
AJY1704	*MatA, prStu2-GFP-STU2, DAD4-mCherry:kan*	Figure 5
AJY838	*MatA, SPC24-GFP:kan. STU2-mCherry:nat*	Figure 5
AJY2163	*MatA, BIM1-GFP:Kan*	Figure 5
AJY2164	*MatA, BIK1-GFP:Kan*	Figure 5
AJY2194	*MatA, SPC25-mCherry:Kan, BIM1-GFP:Nat*	Figure S4
AJY2196	*MatA, NUF2-mCherry:Kan, BIM1-GFP:Nat*	Figure S4
AJY2108	*MatA, prNdc80-GFP-Ndc80, BIM1-mCherry:Hyg*	Figure S4
AJY2195	*MatA, SPC25-mCherry:Kan, BIK1-GFP:Nat*	Figure S4
AJY2197	*MatA, Nuf2-mCherry:Kan, BIK1-GFP:Trp*	Figure S4
AJY2209	*MatA, prNdc80-GFP-Ndc80, BIK1-mCherry:Hyg*	Figure S4
AJY2323	*MatA, STU2-GFP:Kan, SPC97-mCherry:Hyg, pMET3-CDC20:TRP1*	Figure 5
AJY2321	*MatA, BIM1-GFP:Kan, SPC97-mCherry:Hyg, pMET3-CDC20:TRP1*	Figure 5
AJY2322	*MatA, BIK1-GFP:Kan, SPC97-mCherry:Hyg, pMET3-CDC20:TRP1*	Figure 5
AJY2353	*MatA, NUF2-GFP:Kan, SPC97-mCherry:Hyg, pMET3-CDC20:TRP1*	Figure 5
AJY2565	*MatA, STU1-GFP:Kan, SPC97-mCherry:Hyg, pMET3-CDC20:TRP1*	Figure 5
AJY1221	*MatA, DSN1-GFP:kan, SPC25-mcherry:kan*	Figure 6
AJY1223	*MatA, NSL1-GFP:kan, SPC25-mcherry:kan*	Figure 6
AJY1286	*MatA, MTW1-GFP:Kan, SPC25-mCherry:Kan*	Figure 6
AJY1310	*MatA, NNF1-GFP:Kan, SPC25-mcherry:Hph*	Figure 6
AJY1466	*Kan:pgal-GFP-MTW1, SPC25-mcherry:hyg*	Figure 6
AJY1399	*MatA, prDsn1-GFP-DSN1, SPC25-mch:Hyg*	Figure 6
AJY1464	*MatA/Matα, Kan:pgal-GFP-MTW1/Nat:pGal-mCherry-MTW1*	Figure 6
AJY1465	*MatA/Matα, Kan:pgal-GFP-DSN1/Nat:pGal-mCherry-DSN1*	Figure 6
AJY824	*MatA/Matα, NSL1-GFP:kan/NSL1-mCherry:nat*	Figure 6
AJY1138	*MatA/Matα, Spc105-GFP:kanMX6/Spc105-mCherry:His3*	Figure 6

Supplemental Experimental Procedures

Strains and Media

Strains that expressed an essential gene by the galactose promoter (pGal1) were maintained in YP galactose media, as they grew very poorly in glucose media. For FRET measurements, we grew these strains in YP Raffinose media supplemented with empirically determined concentrations of galactose to induce low-level expression (concentrations ranging from 0.05 to 0.3% galactose). The galactose concentrations were chosen such that the average fluorescence signal from the metaphase kinetochore cluster in these strains was equal to that in strains expressing C-terminal fusions of the same subunit from the native promoter. We previously determined that the kinetochore cluster incorporates a very well-defined copy number of each kinetochore complex, even under conditions of over-expression (see ref. [S9] for dosage-invariant incorporation of fluorescently labeled Cse4 molecules and ref. [S2] for the same characteristics for Ndc80). Therefore, the fluorescence signal ensures that the kinetochore clusters incorporate the correct number of molecules for the kinetochore proteins of interest.

For imaging, mid-log phase cells were rinsed and concentrated in synthetic media supplemented with essential amino acids and the appropriate carbon source. Cells were immobilized on ConA coated coverslips and sealed with VALAP to prevent evaporation. Imaging lasted for < 30 minutes.

To depolymerize the spindle, mid-log phase cells were first arrested in G1 using 2 μg/ml α factor and then released into YPD containing 15 μg/ml nocodazole. Cells were imaged ~ 1.5 hours after release into nocodazole. We used strains with pMET3-CDC20 that can be arrested in metaphase to determine the spindle distribution of MAPs. Overnight cultures grown in synthetic media lacking methionine were arrested in G1 as above, and then released into YPD supplemented with excess methionine. Cells were washed and imaged in the presence of excess methionine after 2 hours.

Microscopy

Imaging was conducted on a Nikon Ti-E inverted microscope with a 1.4 NA, 100x, oil immersion objective. The Lumencor LED light engine (472/20 nm for GFP and 543/20 nm or 575/20 nm for mCherry) was used for fluorophore excitation. Filters used for imaging (Chroma) – (1) FRET and high-resolution colocalization: dual-band excitation filter ET/GFP-mCherry (59002x) and excitation dichroic (89019bs), emission-side dichroic (T560lpxr), emission filters: ET525/50m and ET595/50m, (2) Spindle distribution of MAPs: ET-CFP/YFP/mCherry filter set (89002), (3) FRAP: ET-GFP. Images were acquired with an Andor iXon3 EMCCD camera (pixel size 160 nm). For High resolution colocalization and fluorescence distribution and FRAP measurements, 1.5x tube lens was used. A focused Argon-ion laser beam was used for targeted photobleaching in the FRAP experiments. Kinetochore clusters that were separated by ~ 0.8 to 1 μm were designated as metaphase kinetochore clusters, while those separated by > 2 μm were designated as late anaphase/telophase kinetochore clusters [S10].

FRET quantification

Quantification of FRET was conducted using a semi-automated graphical user interface in Matlab [S2]. Briefly, the total fluorescence from kinetochore clusters was measured in the in-focus plane (containing the brightest pixel within the kinetochore cluster image) in all three channels independently. The GFP fluorescence in strains expressing GFP fusions of subunits of Ndc80 and Mtw1 complexes was statistically indistinguishable, as expected [S10]. mCherry fluorescence showed significant variation from strain to strain even for the same kinetochore protein. Since the GFP fluorescence does not change in this

manner, we conclude that the variation in mCherry fluorescence is due to changes either in the brightness or maturation efficiency. We limited variation in the mCherry signal to < 20% about the average by selecting strains exhibiting the highest fluorescence after each yeast transformation. We previously showed that for a fixed number of GFP molecules, the proximity ratio scales linearly with the mCherry number [S2]. However, the observed mCherry variation does not change any of the conclusions based on FRET comparisons. Therefore, we report the uncorrected proximity ratio values.

The fluorescence measured in the FRET channel includes two contaminating signals: GFP bleed-through into the FRET channel and mCherry cross-excitation at the GFP excitation wavelengths. For the imaging conditions used, the GFP bleed-through is 5.8 ± 0.01 % of the signal measured in the GFP channel, while mCherry cross-excitation is 6.1 ± 0.02 % of the mCherry signal [S2]. We used these factors and the GFP and mCherry fluorescence measured for each cluster to estimate the contaminating fluorescence due to GFP bleed-through and mCherry cross-excitation. These fluorescence values were subtracted from the fluorescence measured in the FRET image to obtain sensitized emission, which is the acceptor fluorescence due to FRET. Sensitized emission was then normalized as the proximity ratio:

$$Proximity\ ratio = \frac{Sensitized\ emission}{GFP\ bleed\text{-}through + mCherry\ cross\text{-}excitation}$$

We used the Wilcoxon rank-sum test for all pairwise comparisons of proximity ratios.

Since we hold the fluorophore excitation conditions constant in all experiments, the sensitized emission from the kinetochore cluster is directly related to the number of FRET pairs and to the average FRET efficiency, since we hold fluorophore excitation constant [S2].

High resolution colocalization analysis

Image registration was achieved from images of an immobile 100 nm Tetra-speck bead (Molecular Probes) scanned over the entire image at 0.75 μm interval along X and Y axes. The images of the bead in the GFP and mCherry channel were used to compute the transformation function for registering the mCherry image relative to GFP using the local weighted mean algorithm. Cells expressing GFP and mCherry labeled kinetochore proteins were then imaged by exposing them to GFP and mCherry excitation simultaneously. Excitation intensities were adjusted to obtain sufficiently high signal with a 200 ms integration time. The centroid of each kinetochore cluster was then determined in the GFP and mCherry image by fitting a 10x10 pixel region with a 2-D Gaussian function. The offset between the two centroids was then calculated and corrected for spindle tilt [S3]. The histogram of measured distances was fitted by a non-Gaussian distribution using the maximum likelihood method [S11].

Analysis of fluorescence distribution on the mitotic spindle

10-plane Z stacks were acquired as before using the GFP/mCherry filter cube. Maximum projection image from all ten planes in each stack was used for image analysis as described by [S12]. Briefly, the spindle pole body protein Spc97-mCherry was used to demarcate the two ends of the metaphase yeast spindle. The spindle axis was initially defined by the two brightest pixels in the Spc97-mCherry fluorescence puncta in a mitotic cell, and the image was then rotated to align the spindle axis with the X-axis. Next, a region of interest encompassing the spindle fluorescence was defined as a rectangular area with a height of 11 pixels perpendicular to the spindle axis and also centered on the spindle axis (1 pixel ~ 107 nm). The intensity in each pixel column in this rectangular area was summed. Background correction was obtained from another rectangular region concentric to the signal region and larger in height by 3

pixels. The fluorescence measured in each pixel was then normalized by the cumulative fluorescence from the entire spindle. The spindle lengths in these strains were similar: 1.53 ± 0.21 μm for Bik1 (n=80), 1.51 ± 0.19 μm for Stu2 (n=60), and 1.68 ± 0.28 μm for Bim1 (n=80). The spindle coordinate for each line-scan was normalized with the spindle length and the data was resampled at regular intervals using linear interpolation (Matlab function interp1). Data from the two half-spindles were averaged to display the distribution over one half of the yeast metaphase spindle.

Measurement of the Fluorescence Recovery After Photobleaching (FRAP)

An Argon-Ion laser (Photonics Instruments) was coupled to the microscope light path using the photoactivation port on the microscope body. The laser beam was focused on the sample by the objective through an ET-GFP filter cube. Selected kinetochore cluster was manually aligned in the laser focus and exposed to 488 nm excitation for 100 ms. Due to sub-optimal focusing of the laser beam, the other kinetochore cluster also suffered some photobleaching (see Figure 5B). Immediately after photobleaching, 5-plane Z-stacks (200 nm separation between adjacent planes) were acquired every 15 s for ~ two minutes. Recovery of fluorescence signal in the bleached kinetochore cluster and the decay of fluorescence in the unbleached cluster were both measured using methods discussed above. Each fluorescence recovery and fluorescence decay series was fit with a single exponential to obtain the recovery or decay rates. The half-life was calculated as:

$$t_{1/2} = -\log(1/2)/recovery\ rate$$

Western blot quantification

Western blot quantification was conducted as described previously [S9]. Yeast cells were grown at 25˚C to mid-log phase in YPD. 1 OD600 cells were pelleted and lysed into Laemmli sample buffer (Bio-Rad 161-0737) by repeated vortexing with glass beads (Research Products International Corps#9831) and heating intermittently at 95˚C. Total cell lysates were separated by electrophoresis on 10% SDS-polyacrylamide gels and then transferred to nitrocellulose membranes. The blots were probed with mouse monoclonal antibodies against amino acids 1-238 of GFP (1:1000 Santa Cruz Biotechnology GFP(B-2):sc-9996), followed by peroxidase-conjugated anti-mouse IgG (1:5,000; Sigma, A-4416). Blots were exposed to ECL reagent (Millipore Immobilon Western Chemiluminescent HRP Substrate, WBKLS0100), imaged with UVP ChemiDocIt Gel Imager using VisionWorks LS Software. Band intensities were quantified using “Gel Plot” function in ImageJ.

Supplemental References

S1. Bevington, P.R. (1969). Data Reduction and Error Analysis for the Physical Sciences, (New York: McGraw-Hill).

S2. Joglekar, A.P., Chen, R., and Lawrimore, J.G. (2013). A sensitized emission based calibration of FRET efficiency for probing the architecture of macromolecular machines. Cell and Molecular Bioengineering *6*, 369-382.

S3. Joglekar, A.P., Bloom, K., and Salmon, E.D. (2009). In vivo protein architecture of the eukaryotic kinetochore with nanometer scale accuracy. Curr Biol *19*, 694-699.

S4. Winey, M., Mamay, C.L., O'Toole, E.T., Mastronarde, D.N., Giddings, T.H., Jr., McDonald, K.L., and McIntosh, J.R. (1995). Three-dimensional ultrastructural analysis of the Saccharomyces cerevisiae mitotic spindle. The Journal of cell biology *129*, 1601-1615.

S5. Piston, D.W., and Kremers, G.-J. (2007). Fluorescent protein FRET: the good, the bad and the ugly. Trends in Biochemical Sciences *32*, 407-414.

S6. Censullo, R., Martin, J.C., and Cheung, H.C. (1992). The use of the isotropic orientation factor in fluorescence resonance energy transfer (FRET) studies of the actin filament. Journal of Fluorescence *2*, 141-155.

S7. Wan, X., O'Quinn, R.P., Pierce, H.L., Joglekar, A.P., Gall, W.E., DeLuca, J.G., Carroll, C.W., Liu, S.T., Yen, T.J., McEwen, B.F., et al. (2009). Protein architecture of the human kinetochore microtubule attachment site. Cell *137*, 672-684.

S8. Padilla-Parra, S., Audugé, N., Lalucque, H., Mevel, J.-C., Coppey-Moisan, M., and Tramier, M. (2009). Quantitative Comparison of Different Fluorescent Protein Couples for Fast FRET-FLIM Acquisition. Biophysical Journal *97*, 2368-2376.

S9. Aravamudhan, P., Felzer-Kim, I., and Joglekar, A.P. (2013). The budding yeast point centromere associates with two Cse4 molecules during mitosis. Curr Biol *23*, 770-774.

S10. Joglekar, A.P., Bouck, D.C., Molk, J.N., Bloom, K.S., and Salmon, E.D. (2006). Molecular architecture of a kinetochore-microtubule attachment site. Nat Cell Biol *8*, 581-585.

S11. Churchman, L.S., and Spudich, J.A. (2008). Colocalization of fluorescent probes: Accurate and precise registration with nanometer resolution. In Single-molecule techniques: a laboratory manual, P.R. Selvin and T. Ha, eds. (Cold Spring Harbour, New York: Cold Spring Harbor Laboratory Press), pp. 73-84.

S12. Sprague, B.L., Pearson, C.G., Maddox, P.S., Bloom, K.S., Salmon, E.D., and Odde, D.J. (2003). Mechanisms of microtubule-based kinetochore positioning in the yeast metaphase spindle. Biophys J *84*, 3529-3546.